



Selection and performance of AM superalloys for high-speed flight environments

William Sean James¹ · Supriyo Ganguly¹ · Goncalo Pardal¹

Received: 24 June 2022 / Accepted: 19 August 2022 / Published online: 1 September 2022
© The Author(s) 2022

Abstract

In developing the Wire + Arc Additive Manufacturing (WAAM) process for the manufacture of components used in high-speed flight environments, a selection process for suitable alloys was devised. Using material properties from literature sources, creep-resistant alloys were down-selected based on the requirement for service in a high temperature, high stress environment and the need for an alloy suitable for manufacture using the WAAM process. Down-selected alloys, Inconel 718 (IN718), Rene 41 (RE41), Haynes 188 (H188) and Inconel 625 (IN625), were deposited by a plasma transferred arc WAAM process in an oxygen-controlled environment. Wall structures were built, and samples extracted for mechanical testing. The performance of as-deposited material was then compared against the wrought literature data. Tensile testing at room temperature revealed a performance mismatch, in comparison with wrought literature data, for precipitation strengthened IN718 & RE41; however, this performance mismatch was less significant for solution strengthened H188 and IN625. Results revealed that the AM material did not meet the wrought strength with performance varying depending on each alloy's strengthening mechanism. Results illustrate the need for further processing to return the mechanical performance to wrought values.

Keywords Additive manufacturing · Alloy selection · Mechanical properties · Rene 41 · Inconel 718 · Haynes 188 · Inconel 625

1 Introduction

In this paper, 73 alloys are ranked against the application of a structural component in a high-speed flight environment of short duration (< 1 h), where the external structural component could reach service temperatures of 1200+ K. Representing the environment experienced by a hypersonic flight system, the performance of the components will be optimised for strength at maximum operating temperature. Components for such an application will also be highly stressed to minimise structural mass.

The only group of alloys suitable for this application are creep-resistant superalloys, which are predominantly alloys intended for service at high temperatures which often contain high volumes of Ni and Cr, with a base element other than Fe [1]. The alloys investigated in this study are Ni-based and Co-based superalloys. These materials are alloyed specifically with Cr to offer oxidation resistance which is obtained

through the formation of oxide scale Cr_2O_3 at the component's surface. Traditionally, these alloys have included Ni-, Fe- and Co-based superalloys, which have been specifically developed for high-temperature applications and often boast significant retention of mechanical strength at elevated temperatures and low surface deformation. These alloys often feature a primary austenitic, face-centred-cubic (fcc) matrix, and an array of secondary strengthening phases and carbides to enhance creep resistance. Fe–Ni-based alloys are strengthened by precipitation of intermetallic compounds within the matrix, most commonly by γ' precipitates, but can also be solid-solution strengthened. Ni-based superalloys are mostly strengthened by the precipitation of intermetallic compounds in an austenitic fcc matrix. When Ti and Al are included in the composition, γ' is often the strengthening precipitate. For alloys including Nb, γ'' is also a strengthening precipitate. Ni-based alloys can also be solid-solution strengthened but this is less common. Some Ni alloys, called oxide-dispersion-strengthened alloys, are strengthened by the inclusion of inert particles in the matrix. Co-based alloys are usually strengthened by both solid-solution strengthening and carbides [2, 3].

✉ William Sean James
w.james@cranfield.ac.uk

¹ Welding Engineering and Laser Processing Centre, Cranfield University, Cranfield, Bedfordshire MK43 0AL, UK

An investigation into the effects that the Wire + Arc Additive Manufacturing (WAAM) process has on these alloys was also required, to ensure no adverse effects on the material properties. The WAAM process uses welding power sources and wire as a feedstock to deposit material in a layer-by-layer process [4]. Due to the repetitive layer-by-layer process, WAAM components also undergo a successive heating and cooling cycle which would significantly affect the metallurgical response of an alloy; Xu et al. found a difference in the hardness of WAAM walls deposited from maraging steel, where the bottom of the wall was made harder due to precipitation from the aging effect of the process. They found that the amount of precipitates in the bottom of the wall, i.e. earlier layers, was roughly double the amount found in the top of the wall [4]. Li et al. found, while investigating the deposition of IN625 using WAAM, that this heating cycle was most significant with each 10 successive layers and that beyond 10 layers no significant change in temperature was observed [5].

A large volume of literature exists on alloy selection for a huge variety of applications, each selection method is dependent on application and what the intended use is. The selection of materials for high-speed flight applications is a well explored and continuously developing area; however, most selection processes consider the application only and not the suitability for a preset manufacturing method before the material is found, such various methods examined by Huda and Edi in their review of materials selection for supersonic applications [6]. This selection process is somewhat different in considering not only the end application but also in selecting alloys suitable for the manufacturing process, in this case WAAM.

2 Method

2.1 Alloy selection

An analysis of existing data found in literature was utilised for the purpose of ranking alloys against the application criteria. Several comprehensive sources of data were utilised for this purpose:

- Metallic Materials Properties Development and Standardization (MMPDS-12) [1]
- Superalloys - A Technical Guide by Donachie and Donachie [7]
- Materials Properties Database for Selection of High-Temperature Alloys and Concepts of Alloy Design for SOFC Applications [8]
- High-Temperature High-Strength Nickel-Base Alloys No. 393, Nickel Institute [9]

In addition, respective manufacturer data sheets were utilised, and in some cases where data were otherwise

unavailable, properties were estimated via both interpolation and extrapolation depending on the missing value (estimated figures are indicated in Appendix).

Seventy-three alloys were considered, and each alloy was scored against the chosen criteria, where the highest score indicates the most appropriate choice, and the lowest score indicates the least appropriate alloy. Each alloy was ranked in each category out of a possible maximum of 73. The score from each category was then totalled to give a final rank. The scoring formula is comprised of a series of simplified equations intended to easily identify potentially suitable alloys amongst an extensive list. An example of the mechanical data extracted from literature is included in Fig. 1.

The scoring formula is as follows:

Equation 1 Scoring formular for alloy ranking system.

$$R_{Total} = R.UTS_{1000} + R.UTS_{1400} + R.YS_{1000} + R.YS_{1400} + R.\eta_{W_{1000}} + R.\eta_{W_{1400}} + R.\eta_{B_{1000}} + R.\alpha_{1000} + R.E_{1000} + R.(\alpha \cdot E)_{1000} + R.s \quad (1)$$

$R.X_T$ where R indicates ranked position, X is representing the category (UTS for example) and T is the temperature in °F. UTS is the ultimate tensile strength, YS is the yield strength, α is the coefficient of thermal expansion, and E is the dynamic modulus of elasticity.

Weight efficiency (η_w) also known as specific strength is given by:

Equation 2 Specific strength (weight efficiency).

$$\eta_w = \frac{UTS}{\rho} \quad (2)$$

Specific modulus referred to here as buckling efficiency (η_B) is given by:

Equation 3 Specific modulus (buckling efficiency).

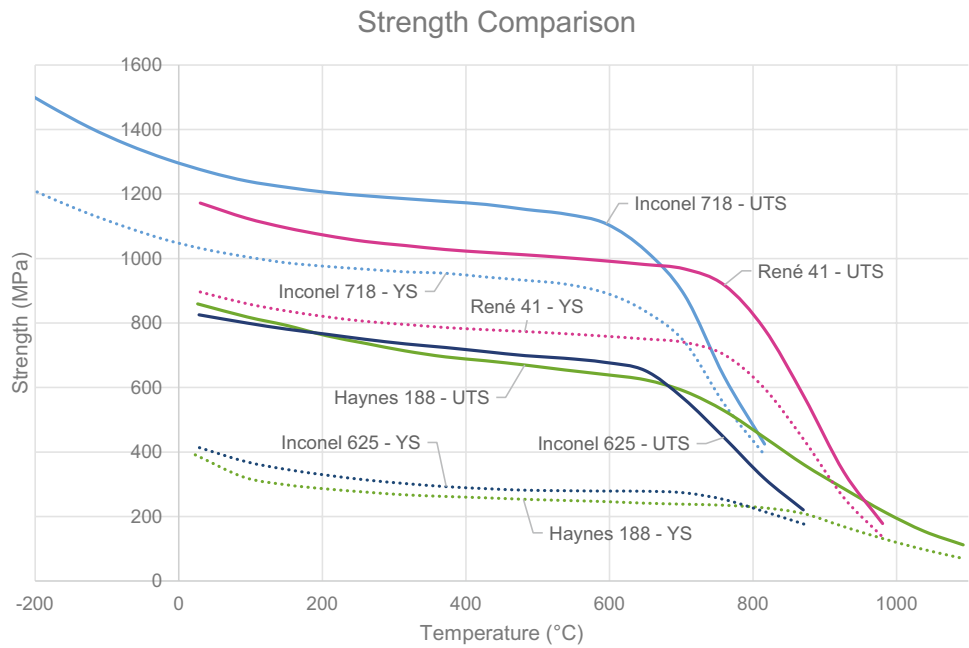
$$\eta_B = \frac{E^{0.5}}{\rho} \quad (3)$$

Susceptibility to post-weld heat treat (PWHT) cracking (s) is given by:

Equation 4 Susceptibility to PWHT cracking. Adapted equation from [10].

$$s = \frac{|k + mx_0 - y_0|}{\sqrt{1 + m^2}} = \frac{|4.5 - Ti_{\%wt} - Al_{\%wt}|}{\sqrt{2}} \quad (4)$$

Fig. 1 Literature data of alloy strength at temperature [1]



The equation of the line in Fig. 2 is given by $y = mx + k$, and the coordinate of each point is given as (x_0, y_0) . The susceptibility to PWHT in Eq. 4 above is a calculation based on Ti and Al content of each alloy and is the distance of the points in Fig. 2 from the ‘increased strain-age cracking’ line indicating the max. content while remaining within the weldable zone. A lower value in this category

represents alloys which are closer to the line, indicating better suitability. Alloys that were significantly above the ‘increased strain-age cracking’ line were excluded from selection. As stated by Donachie and Donachie, Ti and Al are the γ forming elements in nickel superalloys and that when Al + Ti exceeds a critical value PWHT cracking becomes a significant issue for performance [11].

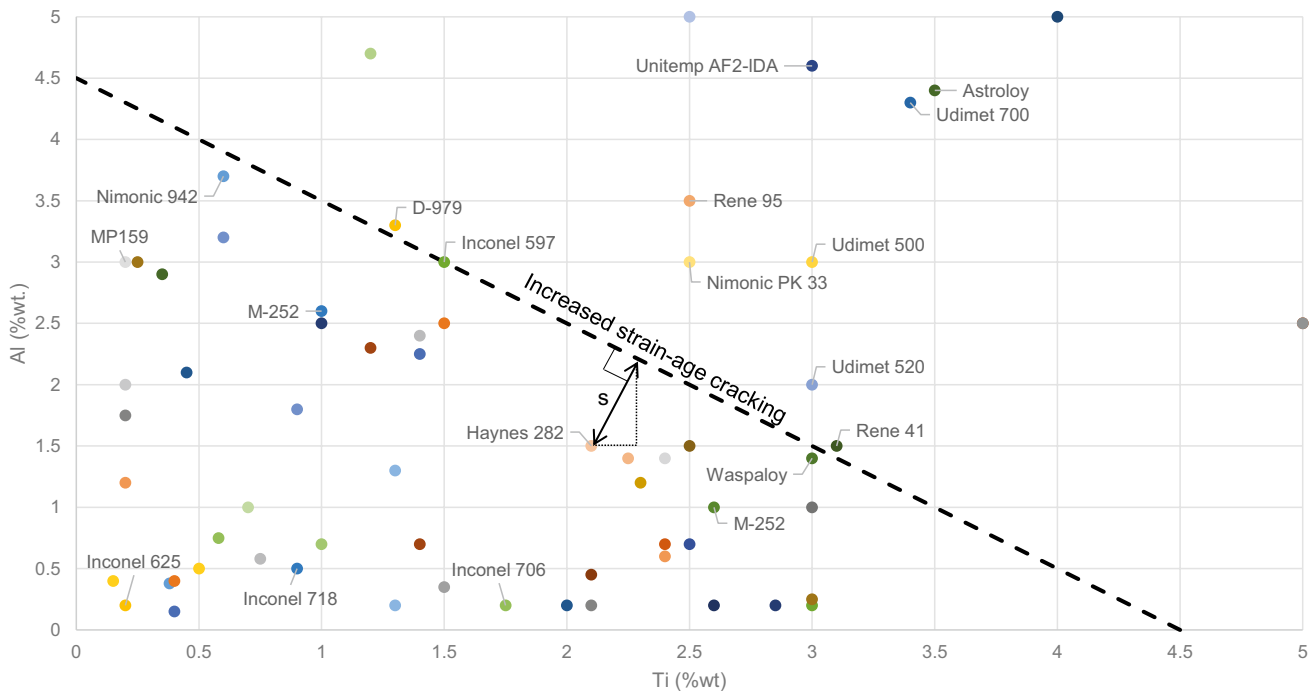
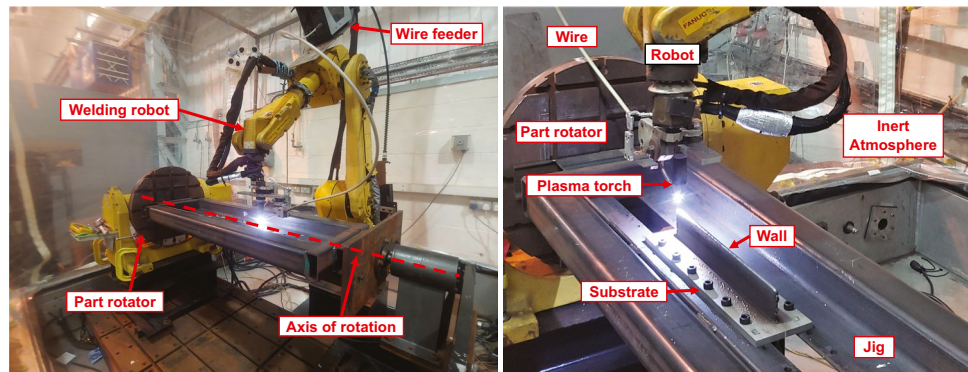


Fig. 2 Diagram of Ti and Al content illustrating weldability of alloys. Adapted from Donachie and Donachie superalloys - a technical guide [11]

Fig. 3 Experimental set-up for WAAM deposition



To select alloys for mechanical testing, the top performing alloy from the alloy selection process, RE41, was down-selected. IN718 was also selected as the alloy has been the subject of previous research using WAAM and is included for comparative purposes due to the alloy having larger volumes of data existing in the literature. H188 was selected to better understand the performance of cobalt-based alloys manufactured using the WAAM system, and IN625 as a solid-solution strengthened Ni-based alloy.

2.2 WAAM deposition

The selected alloys were deposited using a WAAM system consisting of a FANUC six-axis robotic arm, a plasma water-cooled welding torch mounted to the robotic arm, a wire feeder, and a part-rotator - which allowed for WAAM walls to be built on both sides of the substrate plate.

The WAAM deposition process took place inside of an inert enclosure, which provided an argon atmosphere of less than 800 ppm of oxygen and was monitored using an oxygen analyser. The experimental set-up is shown in Fig. 3.

Wall structures were deposited from commercially available wires on both sides of a 10-mm-thick Inconel 718 substrate plate. The composition of the welding wires is given in Table 1 and welding parameters in Table 2. The welding parameters vary in accordance with the wire diameter; in order to maintain a similar deposition rate across the alloys, the wire feed speed was adjusted accordingly.

Table 1 Composition of welding wires (% weight)

Inconel 718													
Ni	Cr	Fe	Nb	Mo	Ti	Al	Mn	Si	Cu	C	Others		
53.57	18.56	17.8	5.01	2.87	0.97	0.60	0.10	0.08	0.07	0.04	0.51		
Rene 41													
Ni	Cr	Co	Mo	Ti	Fe	Al	Nb	V	Si	C	Cu	Mn	Others
53.7	18.9	10.2	9.08	3.20	2.72	1.64	0.12	0.12	0.09	0.07	0.04	0.03	0.007
Haynes 188													
Co	Ni	Cr	W	Fe	Mn	Si	C	La	P	Others			
37.12	22.90	22.20	13.90	2.65	0.81	0.22	0.107	0.06	0.011	0.005			
Inconel 625													
Ni	Cr	Mo	Nb	Fe	Ti	Al	Si	Cu	Mn	C	Others		
64.75	22.16	8.79	3.60	0.24	0.19	0.17	0.04	0.02	0.02	0.01	0.006		

2.3 Mechanical testing

For each selected alloy to undergo tensile testing, samples were extracted from the WAAM walls and machined into coupons. The room-temperature (RT) coupon, conforming to ASTM E8(M) sub-size specification, is shown in Fig. 4. Three coupons were tested from each alloy in the build height orientation (vertical direction). Samples were tested at RT, using an Instron 8801 Servo hydraulic Universal Testing System, and tested to failure using ASTM E8(M). Tensile tests used a strain rate of 0.005 min^{-1} until the onset of plastic deformation and thereafter a crosshead speed of 1.6 mm/min. Specimens were extracted from similar locations on the WAAM wall to minimise variation caused by the WAAM aging effect.

2.4 Microstructure

Specimens of each alloy were extracted from the WAAM walls in build direction–thickness cross sections. Specimens were then prepared for metallographic analysis by mounting, grinding, and polishing successively. Samples were then etched to reveal the microstructure using the following etchants:

IN718 – Swab etched with Kalling’s 2 for 10 s.

RE41 – Swab etched with a solution consisting of 3 g CuSO_4 , 80 ml HCl, 20 ml absolute alcohol [12], for 30 s.

H188 – Electrolytically etched in a solution consisting of 5 g oxalic acid, 95 ml HCl, using 6 V DC with a

Table 2 Welding parameters

	IN718	RE41	H188	IN625
Wire diameter (mm)	1.2	1	1.14	1.2
Torch to work distance (mm)	8	8	8	8
Current (A)	180	180	180	180
Wire feed speed (m/min)	1.8	2.4	2	1.8
Travel speed (m/min)	0.3	0.36	0.36	0.3
Inter-pass temperature (°C)	170	170	170	170

carbon cathode and a stainless anode probe, for 1–2 s [13].

IN625 – Swab etched with aqua regia [14] for 10 s.

3 Results

3.1 Alloy selection

The top five alloys and their score in each category are given in Table 3, as well as the scores of each of the selected alloys (RE41, IN718, H188, IN625).

As can be seen in Table 3, there is not a significant difference in total score between most of the alloys presented. Alloys MP159 and H188 could not be ranked in the susceptibility to cracking category due to both alloys lacking Al and Ti in their composition. In fact, no cracking was visually observed in H188 samples.

3.2 Mechanical testing

The results of tensile testing are given in Table 4 and Fig. 5, where wrought (Wro) values are presented alongside testing results for as-deposited (AD) samples. The data show a mismatch with the wrought data from literature, with AD samples performing somewhat behind the wrought values. The best UTS performance was achieved by RE41 where the performance was 72% of the wrought value, followed by H188, IN625 and IN718, which achieved 69, 64 and 54% of the wrought values, respectively. Comparing the YS performance, there is a correlation between the performance of solid-solution strengthened alloys and the precipitation-strengthened alloys. H188, IN625, RE41 and IN718 achieved 85, 81, 72, and 41% of the wrought YS, respectively.

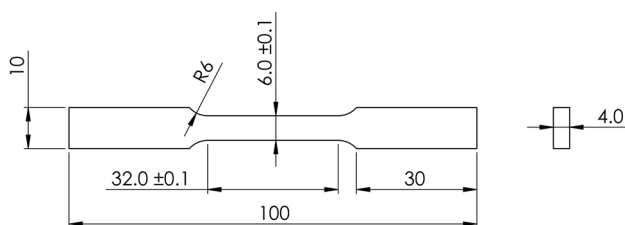


Fig. 4 RT Tensile testing coupon. (Dimensions in mm)

The difference in performance between the alloys could be explained by the differences in strengthening mechanisms. For example, IN718 undergoes an extensive aging process to achieve maximum strength, whereas RE41 although also precipitation strengthened typically undergoes a less extensive treatment, H188 and IN625 are both primarily solid-solution strengthened, which helps to explain why the performance of these alloys more closely resembles the wrought values.

3.3 Microstructure

The microstructure of all four alloys exhibits large columnar grains and a typical solidified dendritic structure for nickel superalloys. In Fig. 6, lighter and darker bands can be observed along the height of the samples, which correlate to the deposited and re-heated material. The curvature of these bands, labelled as ‘remelting line’ in Fig. 6, is mostly curved which is thought to be due to the spreading of molten metal towards the edges during deposition. The difference observed in this spreading is thought to be due to the different viscosities of the alloys and/or slight variations in the deposition process. The grains in RE41 and H188 appear larger although less clearly defined than IN718 and IN625. The grains also extend outward with build height, indicating the flow of heat. In Fig. 6, significant cracking can be observed in IN718 and, to a lesser extent, in RE41, with cracks extending through the layers. No cracking was observed in H188 or IN625.

4 Discussion

The alloy ranking method, although basic, provides an insight into the performance of the alloys in relation to the application. For the high-speed flight environment, performance at elevated temperature such as strength, weight efficiency, and elongation are important factors. The ranking formula (Eq. 1) naturally weights more importance on the alloy’s strength, by having the UTS and YS input into the equation in five separate terms in total, including weight efficiency (specific strength) where UTS is also a term. Although strength is a large factor in the ranking formula, it does include several other factors which are important for high-speed flight, such as density which will affect the overall weight of any components. Elastic modulus and coefficient of thermal expansion are also used on the basis that they will largely dictate the deformation and corresponding thermal stress that any component will experience under high levels of service loading at an elevated temperature. Finally, components are ranked on their suitability for welding, which eliminates any alloys that would experience a large degree of strain age cracking as a result of welding. The volume of Ti and Al in the matrix of precipitation-hardened alloys is a factor in how susceptible the alloy will be to strain-age cracking. As the alloys are effectively heated at and beyond

Table 3 Ranking of alloys

Designation	Total Score	UTS		YS		η_w		η_B	α	E	Stress (α -E)	Cracking
		1000 F	1400 F	1000 F	1400 F	1000 F	1400 F					
Rene 41	673	67	66	63	66	68	66	41	65	37	64	70
MP159	608	71	70	72	72	71	71	35	25	51	15	55
MP35N	593	72	72	71	71	73	73	54	25	72	8	(2)
M-252	591	56	58	46	51	57	57	36	69	30	68	63
Inconel 617	567	19	42	19	25	21	43	48	111	64	111	64
Inconel 718	560	61	59	66	54	61	59	26	50	26	57	41
Inconel 625	314	36	30	26	29	35	31	24	20	37	18	28
Haynes 188	280	25	37	20	23	22	35	1	37	22	56	(2)

their aging temperature during deposition, they precipitate γ' particles during the process affecting the ductility during the process [11]. Interestingly, six of the studied alloys were eliminated due to weldability concerns that otherwise would have appeared within the top 10. This indicates that the majority of superalloys with high strength at temperature are both susceptible to cracking during welding and contain high volumes of Al and/or Ti. To further understand the effect that the WAAM process has on the microstructure and fracture methods, this will be the subject of a future article.

The microstructure of the alloys is observed in Fig. 6. The darker and lighter banding seen in the alloys was also observed by Seow et al. in WAAM built IN718; their opinion agreed that the banding is the appearance of newly deposited and re-heated material [16]. Seow et al. also observed the epitaxial growth of grains upwards and outwards towards the edges of the samples, which was suggested is due to the slight thermal gradient created by the increased cooling experienced at the edges of the deposition [16]. The viscosity difference in the molten alloy could explain the difference observed in the curvature of the remelting lines in Fig. 6. In a study of the melt pool dynamics in laser powder bed fusion using IN718, Ahsan et al. found that fluid flows on the sides of the melt pool due to the high temperature gradient and that the pool expands in both x and y due to Marangoni convection, buoyancy, and recoil pressure [17]. This explains the curved appearance, although further investigation is required to

establish if a difference in viscosity is responsible for the differing shapes seen across the four alloys.

The strengthening mechanisms of each alloy are somewhat different but fall into two distinct categories. IN718 and RE41 are precipitation-hardened alloys, whereas H188 and IN625 are solid-solution strengthened alloys. H188 is the only alloy included that is Co-based; however, it is alloyed significantly with Ni and Cr. H188 is not hardenable except through cold working, and its strength is derived through its solid-solution strengthened fcc matrix [18]. IN625 was also designed as a solid-solution strengthened alloy; however, the alloy has been observed to be subject to precipitation of intermetallic phases and carbides [19]. RE41 is strengthened by the precipitation of phases within its matrix, and intermetallic phase γ' is the main strengthening phase and forms with Ni, Al and/or Ti [20]. IN718 is also strengthened primarily by γ' phases but is also strengthened by precipitation of γ'' phases, which forms from Ni and Nb [21]. Some correlation can be observed in the tensile results; between the level of precipitation hardening the alloy is ordinarily subjected to and the shortfall in performance of AD material. With less age-hardenable alloys experiencing the least decline in performance due to the WAAM process.

The difference in cracking observed between the alloys is thought to be related to the precipitation hardening of the alloys, with the most hardenable alloy, IN718, experiencing the most cracking, followed by RE41, whereas the other less age hardenable alloys IN625 and non-hardenable H188 did not experience any cracking. This cracking could also be responsible for the larger shortfall in tensile performance observed in IN718 and RE41.

To increase the strength of the alloys further, an inter-pass cold working process could be included in the WAAM process, combined with a post-deposition heat-treatment, which will be investigated in a future article. A previous study by Xu et al. found that cold rolling IN718 after each layer deposited increased the strength to meet and in some cases exceed the wrought performance [21]. The difference observed between the AD samples and the wrought strength highlights the need for additional processing of the alloys, such as post-process heat-treatments and/or mechanical working to return to wrought

Table 4 RT Mechanical results and comparison with wrought (Wro) literature data [15]

Alloy	Condition	UTS (MPa)	0.2 % YS (MPa)	Elongation (%)
IN718	Wro	1435	1185	21
	AD	774.30	485.33	23.90
RE41	Wro	1420	1060	14
	AD	1017.40	764.00	26.16
H188	Wro	960	485	56
	AD	660.89	412.00	56.26
IN625	Wro	965	490	50
	AD	622.21	396.97	57.26

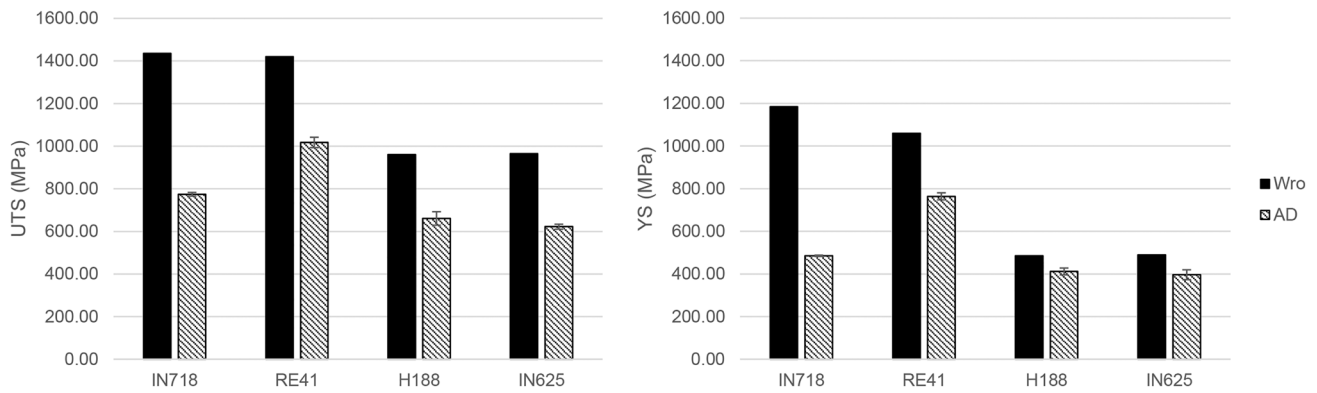


Fig. 5 Graphical representation of data presented in Table 4

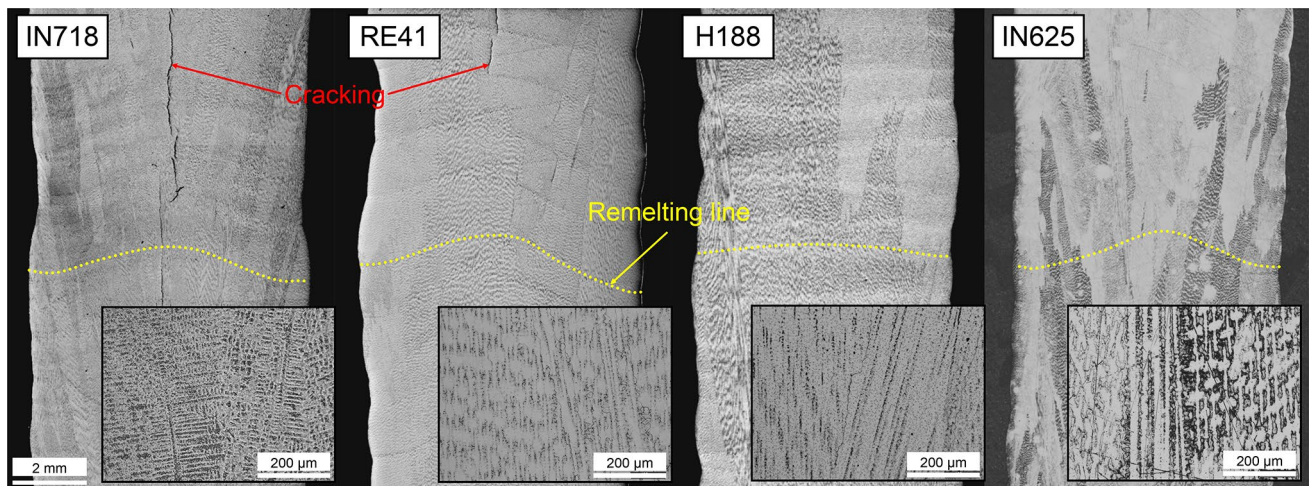


Fig. 6 Microstructure of as-deposited alloys

performance. Precipitation of secondary phases at the grain boundary is one of the main sources of strength for precipitation-strengthened alloys. In a previous study on IN718 by Xu et al., it was suggested that the presents of large columnar grains in the WAAM structure make the precipitation of these phases less likely, due to the reduced grain boundary area [22]. This makes the use of a mechanical process to disrupt the large WAAM grains a necessity to achieve peak strength.

Further research is required to establish processing methods which can return WAAM-deposited creep-resistant alloys to their wrought performance.

5 Conclusions

In conclusion, suitable alloys for the high-speed flight application were identified using a scoring method. The method was calculated using material properties from literature sources, input into a series of simplified equations. The selected alloys then underwent mechanical testing after

WAAM deposition, to understand the AD performance of the alloys compared with the wrought data from literature.

The study found:

1. Alloy RE41 is the most suitable alloy for both WAAM deposition and for application in high temperature–high stress environments.
2. Mechanical testing shows a similarity between precipitation strengthened alloys (RE41 & IN718), where these AD alloys significantly underperformed compared to wrought material. Solid-solution strengthened alloys (H188 & IN625) also underperformed but the difference was less significant.
3. WAAM deposition of solid-solution strengthened alloys, H188 and IN625 achieves a YS performance closer to the wrought values.
4. WAAM deposition of precipitation strengthened alloys can result in significant cracking, which is not experienced when depositing solid-solution strengthened alloys.
5. Additional investigation is required into methods of returning WAAM superalloys to their wrought strength.

Appendix: sample of mechanical properties from literature

Designation	Score	Form	Density kg/m ³	UTS (MPa)			YS (MPa)			Tensile elongation (%)		
				21 °C	538 °C	760 °C	21 °C	538 °C	760 °C	21 °C	538 °C	760 °C
Nickel base												
Inconel 617	260	Bar	8360	740	580	440	295	200	180	70	68	84
Inconel 625	304	-	8440 [9]	965	910	550	490	415	415	50	50	45
Inconel 718	557	Bar	8220	1435	1275	950	1185	1065	740	21	18	25
M-252	587	Bar	8250	1240	1230	945	840	765	720	16	15	10
Rene 41	703	Bar	8250	1420	1400	1105	1060	1020	940	14	14	11
Cobalt base												
Haynes 188	280	Sheet	8980	960	740	635	485	305	290	56	70	43
MP35N	588	Bar	8410	2025	(1773)	(1548)	1620	(1430)	(1415)	10	-	-
MP159	594	Bar	8330*	1895	1565	(1340)	1825	1495	(1480)	8	8	-

Designation	Mean coefficient of thermal expansion α (10 ⁻⁶ K)	Dynamic modulus of elasticity E		Content (%wt)	
		21 °C	538 °C	Al	Ti
Nickel base					
Inconel 617	13.9	210	176	1	0
Inconel 625	15.3 [8]	208 [9]	179 [9]	0.2	0.2
Inconel 718	14.4	200	171	0.5	0.9
M-252	13.0	206	177	1	2.6
Rene 41	13.5	220 [9]	191 [9]	1.5	3.1
Cobalt base					
Haynes 188	14.8	207	192 [9]	0	0
MP35N	(15.3)	231	(192)	0	0
MP159	15.1 [9]	206 [9]	(167)	0.2	3

Data from Donachie Superalloys – A Technical Guide [15], unless otherwise specified

(Extrapolated/ interpolated values are shown in parentheses)

*Manufacturers data

Acknowledgements The authors wish to acknowledge the UK Ministry of Defence for their financial support, and the industrial supervisors from DSTL Porton Down, for their ongoing advice and guidance: Mr Graham Simpson, Dr Sarah Baker, and Dr Matthew Lunt.

Funding This work was funded by the Defence Science & Technology Laboratory, UK (DSTL).

Data availability The raw/processed data required to reproduce these findings cannot be shared at this time as the data also form part of an ongoing study.

Code availability Not applicable.

Declarations

Ethical approval In the author's opinion, there are no ethical issues with the research presented in this paper. The authors confirm this manuscript has not been published elsewhere and is not under consideration by another journal.

Consent to participate Not applicable.

Consent to publication All authors consent to the publication of this paper.

Conflict of interest The authors declare no competing interests.

Open Access This article is licensed under a Creative Commons Attribution 4.0 International License, which permits use, sharing, adaptation, distribution and reproduction in any medium or format, as long as you give appropriate credit to the original author(s) and the source, provide a link to the Creative Commons licence, and indicate if changes were made. The images or other third party material in this article are included in the article's Creative Commons licence, unless indicated otherwise in a credit line to the material. If material is not included in the article's Creative Commons licence and your intended use is not permitted by statutory regulation or exceeds the permitted use, you will need to obtain permission directly from the copyright holder. To view a copy of this licence, visit <http://creativecommons.org/licenses/by/4.0/>.

References

- Battelle Memorial Institute (2017) Heat-resistant alloys. In *Metallic Materials Properties Development and Standardization (MMPDS-12)*. Battelle Memorial Institute. Available at: <https://app.knovel.com/hotlink/pdf/id:kt00CX2NX1/metallic-materials-properties/metallic-m-mechanical>
- Donachie MJ, Donachie SJ (2002) Understanding superalloy metallurgy. In *Superalloys - A Technical Guide*. 2nd edn. ASM International, pp 25–39. <https://doi.org/10.31399/asm.tb.stg2.t61280025>
- Yang Z, Weil KS, Paxton DM, Stevenson JW (2003) Selection and evaluation of heat-resistant alloys for SOFC interconnect applications. *J Electrochem Soc* 150(9):A1188. <https://doi.org/10.1149/1.1595659>
- Xu X, Ganguly S, Ding J, Guo S, Williams S, Martina F (2018) Microstructural evolution and mechanical properties of maraging steel produced by wire + arc additive manufacture process. *Mater Charact*. Elsevier. 143:152–162. <https://doi.org/10.1016/j.matchar.2017.12.002>
- Li S, Li JY, Jiang ZW, Cheng Y, Li YZ, Tang S, Leng JZ, Chen HX, Zou Y, Zhao YH, Oliveira JP, Zhang Y, Wang KH (2022) Controlling the columnar-to-equiaxed transition during Directed Energy Deposition of Inconel 625. *Add Manuf* 57(January). <https://doi.org/10.1016/j.addma.2022.102958>
- Huda Z, Edi P (2013) Materials selection in design of structures and engines of supersonic aircrafts: A review. *Mater Des*. Elsevier Ltd. 46:552–560. <https://doi.org/10.1016/j.matdes.2012.10.001>
- Donachie MJ, Donachie SJ (2002) *Superalloys - a technical guide*. 2nd edn. ASM International. Available at: <https://app.knovel.com/hotlink/toc/id:kpSATGE003/superalloys-technical/superalloys-technical>
- Yang ZG, Stevenson JW, Paxton DM, Singh P, Weil KS (2002) Materials properties database for selection of high-temperature alloys and concepts of alloy design for SOFC applications. Pacific Northwest National Laboratory. <https://doi.org/10.2172/15010553>
- INCO (2020) High-temperature high-strength nickel-base alloys no. 393. Available at: https://nickelinstitute.org/media/8d93486143182f5/nickel_incopub393_updated-june-2021.pdf
- Larson R, Hostetler R (2007) *Trigonometry*, 7th edn. Houghton Mifflin, Boston, MA
- Donachie MJ, Donachie SJ (2002) Joining technology and practice. In *Superalloys - A Technical Guide*. 2nd edn. ASM International, pp 65–78. Available at: <https://app.knovel.com/hotlink/pdf/id:kt008GQY5K/superalloys-technical/joining-superalloys>
- Li J, Wang HM, Tang HB (2012) Effect of heat treatment on microstructure and mechanical properties of laser melting deposited Ni-base superalloy Rene'41. *Mater Sci Eng, A* 550:97–102. <https://doi.org/10.1016/j.msea.2012.04.037>
- Middleton LA, Kennon NF, Dunne DP, South N (1985) Metallographic preparation. *Metallography* 17:51–59
- Xing X, Di X, Wang B (2014) The effect of post-weld heat treatment temperature on the microstructure of Inconel 625 deposited metal. *J Alloys Compd*. Elsevier B.V., 593, pp 110–116. <https://doi.org/10.1016/j.jallcom.2013.12.224>
- Donachie MJ, Donachie SJ (2002) Selection of Superalloys. In *Superalloys - A Technical Guide*. 2nd edn. ASM International, pp 11–24. Available at: <https://app.knovel.com/hotlink/pdf/id:kt008GQU1/superalloys-technical/superalloy-forms>
- Seow CE, Coules HE, Wu G, Khan RHU, Xu X, Williams S (2019) Wire + arc additively manufactured inconel 718: Effect of post-deposition heat treatments on microstructure and tensile properties. *Mater Des*. Elsevier Ltd 183:108157. <https://doi.org/10.1016/j.matdes.2019.108157>
- Ahsan F, Razmi J, Ladani L (2022) Global local modeling of melt pool dynamics and bead formation in laser bed powder fusion additive manufacturing using a multi-physics thermo-fluid simulation. *Progress in Additive Manufacturing*. Springer International Publishing (0123456789). <https://doi.org/10.1007/s40964-022-00302-w>
- Herchenroeder RB (1968) Haynes alloy no. 188 aging characteristics. In *International Symposium on Structural Stability in Superalloys*. Seven Springs, PA, pp 460–500. https://doi.org/10.7449/1968/superalloys_1968_460_500
- Shankar V, Rao KB, Mannan SL (2001) Microstructure and mechanical properties of Inconel 625 superalloy. *J Nucl Mater* 288(2–3):222–232. [https://doi.org/10.1016/S0022-3115\(00\)00723-6](https://doi.org/10.1016/S0022-3115(00)00723-6)
- Kaufman M (1963) Control of phases and mechanical properties in nickel-base alloys of rene 41 type. *Transactions of the Metallurgical Society of AIME* 227(2):405
- Xu X, Ganguly S, Ding J, Seow CE, Williams S (2018) Enhancing mechanical properties of wire + arc additively manufactured INCONEL 718 superalloy through in-process thermomechanical processing. *Mater Des*. Elsevier Ltd 160:1042–1051. <https://doi.org/10.1016/j.matdes.2018.10.038>
- Xu X, Ding J, Ganguly S, Williams S (2019) Investigation of process factors affecting mechanical properties of INCONEL 718 superalloy in wire + arc additive manufacture process. *J Mater Process Technol*. Elsevier 265:201–209. <https://doi.org/10.1016/j.jmatprotec.2018.10.023>

Publisher's Note Springer Nature remains neutral with regard to jurisdictional claims in published maps and institutional affiliations.